EVIDENT

14

Tribology

Surface Interaction Experiments

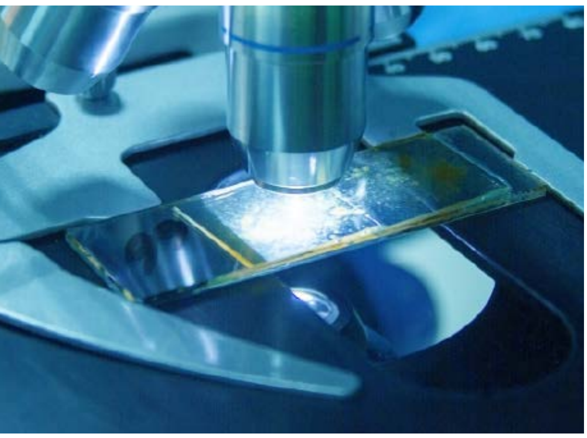

OLYMPUS®

WILEY

Contents

3 Introduction
Tribology: Surface interaction experiments

5 Tribological behavior of polymer/metal composites having a sandwich structure
Adapted from Zhang *et al.*

11 Ultra-high-molecular-weight polyethylene: Abrasive wear behavior in a rotating lubricated environment
Adapted from Sun *et al.*

19 Tribology and compressive creep of polytetrafluoro-ethylene/nickel-titanium composites
Adapted from Li *et al.*

26 Case Study: Getting up to scratch with Croda – testing anti-scratch additives for polymer plastics
Sarah Williams

Imprint

© Wiley-VCH GmbH
Boschstr. 12,
69469 Weinheim, Germany
Email: info@wiley-vch.de
Editors:
Dr. Cecilia Kruszynski &
Róisín Murtagh

01 Tribology: Surface interaction experiments

Tribology, derived from the Greek word *tybos* meaning rubbing, is the science of studying the interaction of moving surfaces. Since its introduction in 1964, the concept of tribology has been used to explain how humans have been able to move and manipulate large objects for centuries; this includes ancient civilizations in Egypt and China who used lubrication principles to move heavy stones used in their monumental structures.

Tribology investigates the wear, friction, and lubrication of surfaces and the associated design elements of related mechanical components. Its purpose is to explore the friction characteristics and wear response of contending surfaces in motion. This interdisciplinary topic necessitates the collaborative efforts of researchers from a wide range of disciplines, including mechanical, chemical, and biomedical engineering, materials science, chemistry, physics, mathematics, computer science, and more.

Tribology has traditionally been applied to the most common sliding components such as bearings, gears, brakes, and seals in machinery used for sliding or rotating motion. In recent years, tribology has taken on an even more important role as it focuses on the efficient consumption of energy and the development of lubricants that will reduce carbon dioxide emissions in transport media. Tribology is also applicable in other industries such as metal machining operations, where it can enable increased productivity and reduced costs. Additionally, nanotribology, which studies tribological phenomena at the nanoscopic level, has been gaining traction due to the invention of the atomic force microscope. This has opened up a wide horizon of new applications and research opportunities.[1]

Friction, wear, and lubrication are the key components of tribology. Friction is the resistance to motion, which varies in intensity depending on the materials, geometry, and surface characteristics of the two bodies in contact, as well as the operating conditions and environment. Generally, friction increases with higher load and surface roughness, which can be reduced by the application of a lubricant. Wear, on the other hand, is the loss of materials due to sliding and is undesirable as it increases friction and can cause component failure. Lubrication is used to reduce friction and wear between two surfaces by separating them, so they are not in direct contact. Lubricants also provide other functions such as carrying heat and contaminants away from the interface; they can be liquids, gases, or solids depending on the application.

Testing the tribological properties of materials usually involves setting up complete systems to perform specialized tests, such as field, bench, component, and model tests.[2] Model tests such as measurements of lubricant film thickness, friction, and wear are

back to content

essential in tribology. Electrical and interferometric methods can also be used; however, it is important to remember that tribology tests should be tailored to their intended purpose. Furthermore, the evaluation of sliding surfaces through conventional and electron microscopes, along with the quantification of wear and friction, gives valuable insight into the friction and wear mechanisms, which can then be used to improve the service life of mechanical pieces, prevent failures, and ultimately reduce costs and carbon emissions.

Therefore, tribology is a vital component in industrial progress, innovation, and development. Tribological testing is essential to gain a better understanding of the failure mechanisms of mechanical components and their capabilities.

REFERENCES

[1] *Bhushan, B., Israelachvili, J.N., and Landman, U. (1995) Nanotribology: friction, wear and lubrication at the atomic scale. Nature, 374 (6523), 607–616.*

[2] *Meng, Y., Xu, J., Jin, Z., Prakash, B., and Hu, Y. (2020) A review of recent advances in tribology. Friction, 8 (2), 221–300.*

back to content

02 Tribological behavior of polymer/metal composites having a sandwich structure

Adapted from Zhang *et al.*, 2021

Polytetrafluoroethylene/metal mesh composites with a sandwich structure were prepared using layer-press technology. The influence of the mesh structure and mesh density of the middle metal layer on the tribological properties of composites were researched in detail.

Polymer composites have been widely utilized in automotive, aerospace, and a diversity of other fields [1,2] due to their suitable mechanical and tribological properties. Polytetrafluoroethylene (PTFE), the typical self-lubricating polymer with a low friction coefficient and high chemical resistance and thermal stability [3], is the representative material among these composites and has been widely used. Unfortunately, the poor abrasion resistance and low load-carrying capacity always restrict its widespread application in sophisticated equipment.[4]

Metal fillers have been extensively added to polymers to improve their abrasion resistance, load-carrying capacity, and thermal conductivity.[5–7] Particle and fiber additives can also be used to improve composites' mechanical properties and load-bearing capacity. Due to the strong interface bonding between fibers and a polymer matrix, the composites can be largely enhanced.[8,9] It is well known that mesh structures have the advantage of simple preparation, high strength, and location restriction.[10,11] However, most of the research on sandwich structure composite materials is reflected in improving mechanical properties; there are few reports about the applications of mesh structures in friction materials.

In this study, we focus on preparing and studying a type of new PTFE composite with a sandwich structure. The PTFE/metal mesh composites were prepared using layer-press technology, and their tribological performances are detailed below.

EXPERIMENT

Preparation of sandwich PTFE composites

The size of PTFE powders is 1–3 μm (Daikin M18F). The different metal meshes (Anping Metal Mesh, China, **Figure 1**) were used as the middle layer of composites. All the metal wire materials were made of 304 stainless steel.

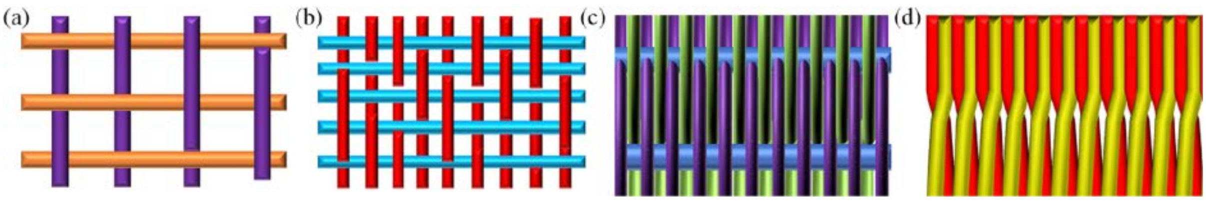

Figure 1: Schematic diagram of metal mesh: (a) 200#PW, (b) 500#PW, (c) 500#PWD, (d) 1000#TWD.

back to content

Table 1: Test conditions for UMT-5

Test conditions	Load (N)	Reciprocating frequency (Hz)
1	20	10
2	20	20
3	30	10
4	30	20

For composite fabrication, 0.3 g of PTFE was added into a cylindrical mold with a diameter of 20 mm, which acted as the bottom layer of the sandwich composite. Then, the metal mesh was placed on the top of the bottom PTFE used as the middle layer of the sandwich composite. Then, 0.3 g of PTFE was put into the mold as the upper layer. Finally, the composites were cold-pressed for 10 min under a cold-pressed pressure of 50 MPa. Next, the cold compressed specimens were sintered with a muffle furnace (ca. 375 °C (698 °F), 300 min). After heating, the sample was placed into the mold for flattening with a cold-pressed pressure of 10 MPa. The obtained sandwich PTFE composites were named according to their metal mesh. For example, PTFE-200#PW represents the middle layer as the metal mesh with a 200# plain woven structure.

Characterization of tribological performance

The friction coefficient (COF) of composites was tested by a ball-on-disc tribometer (UMT-5, CETR). The PTFE composites were polished with 3000# abrasive paper prior to the test. The diameter of the GCr15 stainless ball was 10 mm. The friction test conditions are shown in **Table 1** and all testing times were 60 min. At the end of each test, the dimensions of the wear scar of samples were measured with a 3D surface measuring instrument (OLS5000, Olympus, accuracy: ca. 1 nm). Finally, the wear rate (ε) was calculated using Equation 1: [12]

$$\varepsilon = \upsilon/(F \cdot L) \qquad (1)$$

where F is the applied normal load (N), and L is the total sliding distance of the sample (m).

The thermal conductivity of composites was characterized by a thermal conductivity tester (DRL-III, Deshe Precision Instruments) and compared with that of neat PTFE, for which the composites were cut into samples with a diagonal length of 30 mm and a thickness of 3 mm.

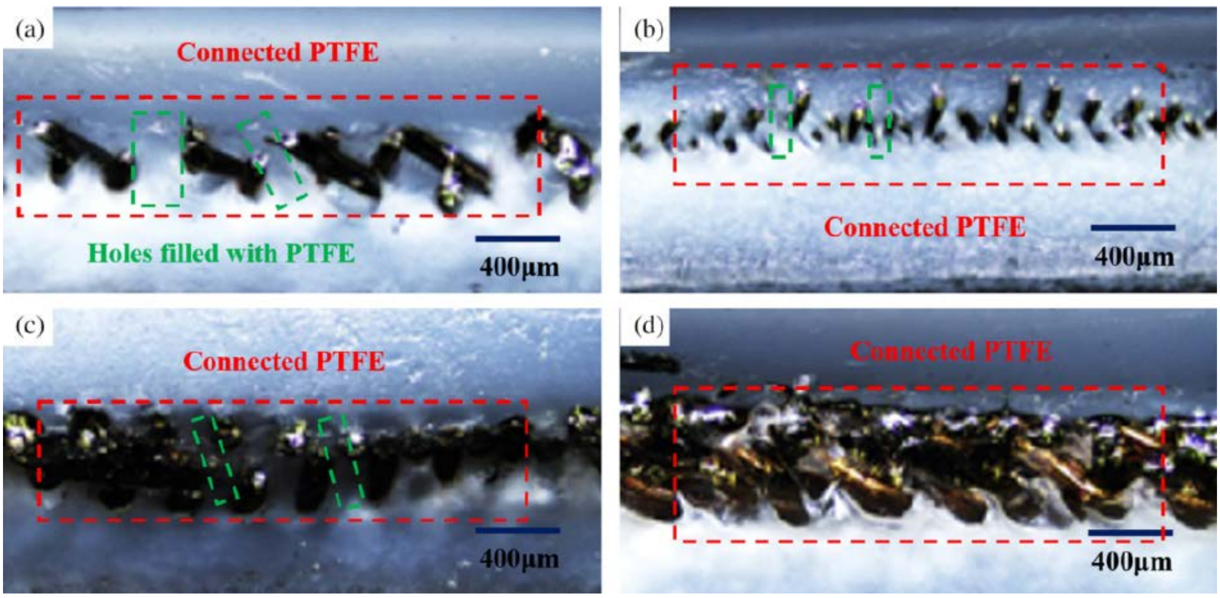

Figure 2: Cross-section morphology of sandwich PTFE composites: (a) PTFE-200#PW, (b) PTFE-500#PW, (c) PTFE500#-PWD, (d) PTFE-1000#TWD.

back to content

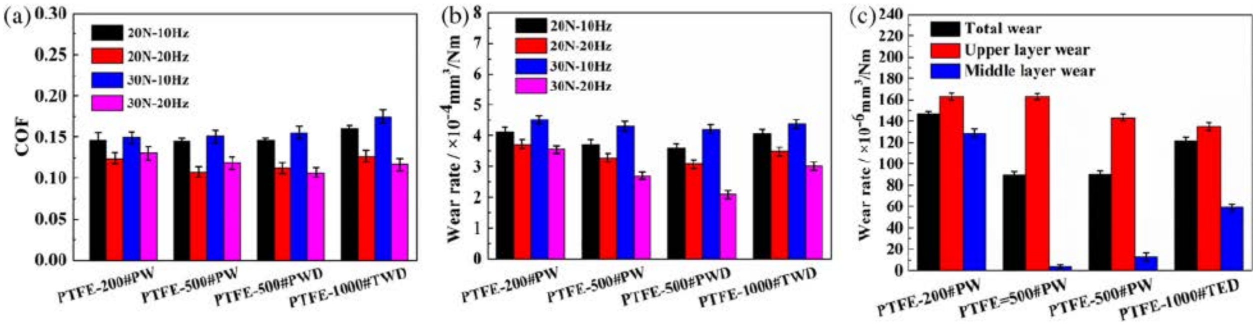

Figure 3: (a) The average COFs of sandwich PTFE composites, (b) the wear rates of sandwich PTFE composites, (c) segmented the wear rate of sandwich PTFE composites under "30 N-20 Hz".

Furthermore, in order to observe and characterize the morphology of sandwich PTFE composites, metal mesh constructions, and wear tracks, a 3D surface measuring instrument (OLS5000, Olympus) and a scanning electron microscope (Quanta 200, FEI) equipped with an energy dispersive X-ray spectroscopy (EDS) at an accelerating voltage of 15 kV were utilized.

RESULTS AND DISCUSSION

The morphology of sandwich PTFE composites

All metal mesh surfaces are uneven with regular raised areas. 200#PW and 500#PW have the same mesh structure, the latter being more compact. Two typical metal mesh structures were used, the plain woven Dutch and the twill-woven Dutch. **Figure 2** shows the cross-section images of sandwich PTFE composites. The thickness of the upper PTFE layer is about 0.6 mm. Under the effect of the compressed pressure, the PTFE can fill into the holes of metal meshes. PTFE of the upper layer and the bottom layer can connect in composites with 200#PW, 500#PW, and 500#PWD, as shown in **Figures 2a-c**.

Tribological performance of composites

All COFs ranged from 0.107 to 0.175 (**Figure 3a**). The COFs of composites tested at 10 Hz increased with testing time and with friction load. Moreover, the bigger the friction frequency, the smaller the COF. The mesh density has little influence on the COF (PTFE-200#PW and PTFE-500PW) when the friction frequency is 10 Hz. The COF of composites with PWD and TWD metal mesh is higher than that of PW metal mesh at the friction load of 10 N. Moreover, PTFE500#PWD has the lowest COF value of 0.106 when the friction load is 30 N and friction frequency is 20 Hz, and PTFE-1000#TPW owns the highest COF of 0.175 with the load of 30 N and the frequency of 10 Hz.

Figure 3b shows the wear rates of different composites. The wear rates of the composite tested at 10 Hz are larger than that tested at 20 Hz. It can be attributed to the fact that at 10 Hz the main wear happens on the upper layer of PTFE, while the wear reaches the metal mesh avoiding the wear volume increased at 20 Hz. The wear rate of these composites ranged from 0.9×10^{-4} to 1.67×10^{-4} mm^3/Nm. The higher densities of metal mesh produce lower wear rates. Composite PTFE-500PWD shows the best anti-wear property. When the friction load is 30 N and friction frequency is 20 Hz, the wear rate of composite PTFE-500PWD is the smallest value (9×10^{-5} mm^3/Nm) among these samples. In fact, the wear volume of the sandwich PTFE composites is divided into two parts. The upper layer of PTFE wears seriously and occupies most of the wear volume. When the metal mesh is worn, the sandwich PTFE composites is divided into two parts. The wear volume will be greatly reduced. To more clearly demonstrate that the upper layer of PTFE experiences significant wear and has a major impact on reducing the wear rate through the use of the metal mesh, we recalculated the wear rate and divided it into segments under the "30 N-20 Hz" test conditions. As shown in **Figure 3c**, the wear rate of the middle layer of PTFE-500PW is approximately 50 times lower than that of the upper layer.

back to content

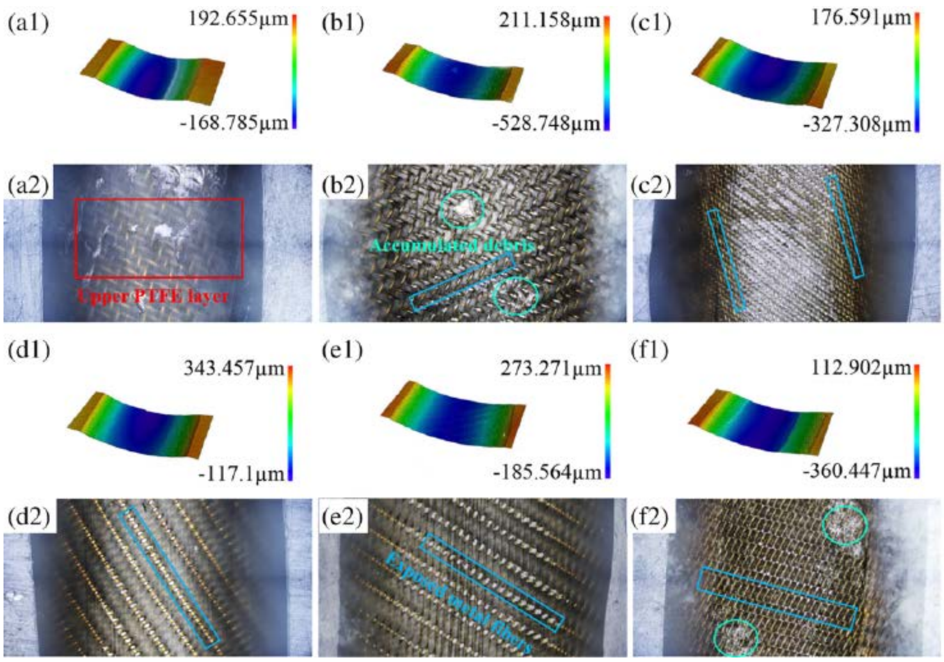

Figure 4: Topography of wear tracks on sandwich PTFE composites. 3D topography of sandwich PTFE composites: (a1) PTFE-200#PW-20 N-10 Hz, (b1) PTFE-200#PW-30 N-20 Hz, (c1) PTFE-500#PW-20 N-20 Hz, (d1) PTFE-500#PWD-20 N-20 Hz, (e1) PTFE-500#PW-30 N-20 Hz, (f1) PTFE-1000#TWD30 N-10 Hz, and Figures 4a2-f2 are their corresponding 2D images.

Figure 4 depicts some typical 2D and 3D images of wear tracks on sandwich PTFE composites, respectively. When the friction load is 20 N and the friction frequency is 10 Hz (**Figures 4a1, 4a2**), there is a lot of wear debris on the wear track of the upper PTFE layer. The middle layer of metal mesh plays an important role in enhancing the strength and reducing the elastic deformation of composites at this stage.[13,14] With the increased friction load or frequency, the upper PTFE layer is worn out, which induced the friction counterpart of the steel ball to contact the middle metal mesh of composites (**Figures 4b1–f1, b2–f2**).

Figure 5 shows the optical images of the counterpart steel balls. When the upper PTFE layer is not worn out, there are no obvious scratches on the surface of the steel balls, and some discontinuous PTFE can be also found (as shown in **Figure 5(a)-(d)**). When the upper PTFE layer is worn out, there are slight wear scratches formed on the steel balls.

On the other hand, the thermal conductivity increased with the addition of metal mesh. A higher density of PW metal mesh can arise a higher thermal conductivity, and the thermal conductivity of composites with PWD and TWD metal mesh is higher than that with PW metal mesh. Moreover, PTFE-1000#TWD obtains the highest thermal conductivity value of 0.31 W/mK, which is 29% higher than that of neat PTFE (0.24 W/mK). Thus, the addition of metal mesh leads to an increase in thermal conductivity for efficiently dissipating frictional heat, which can reduce the adhesive wear caused by friction heat.[7]

Antifriction and antiwear mechanisms of sandwich PTFE composites

The antifriction and antiwear mechanisms of sandwich PTFE composites are shown in **Figure 6**. Firstly, the PTFE is softened due to the friction heat generated.[15] The PTFE will be pulled out and delaminated by the mechanical extrusion, resulting in wear. At this time, the middle layer of the metal mesh and PTFE are connected through mesh holes and prevent the PTFE from being ripped from the matrix. In addition, the metal mesh can play an important role in enhancing the strength and reducing the elastic deformation of composites.[13,14] Moreover, the metal mesh in sandwich PTFE composites can increase thermal conductivity, which can reduce the adhesive wear caused by friction heat.[7] Secondly, when the upper PTFE layer is worn out, the exposed metal mesh can restrict the PTFE to a fixed area and prevent it from being pulled off persistently. Thus, the exposed metal mesh is in contact with the steel ball, leading to a smaller contact region. With the aggravation of wear, the middle metal mesh is partly worn, and the bottom PTFE will be squeezed into the friction area under the frictional load. The small contact region can reduce the adhesion of PTFE to the steel ball, resulting in a sudden decrease of COF (**Figure 3**) and a stable COF.

back to content

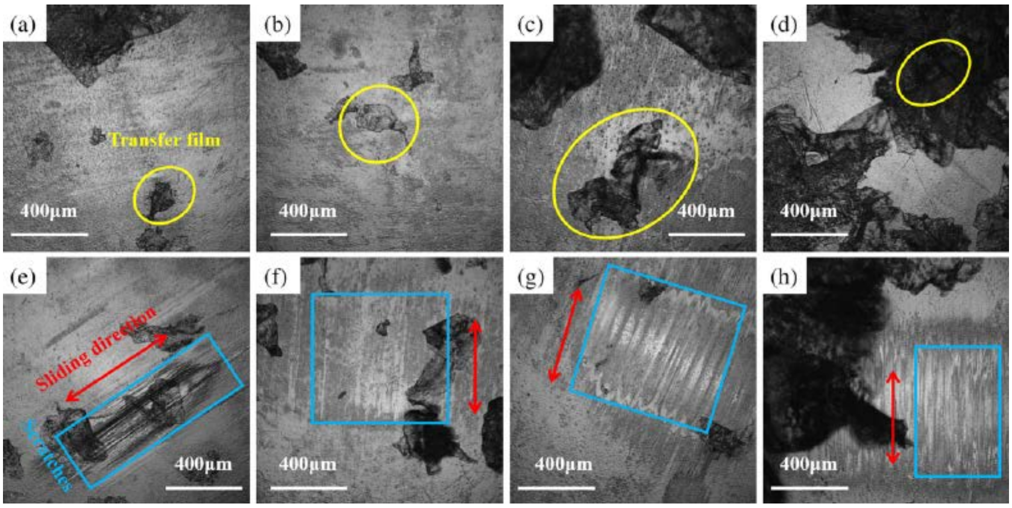

Figure 5: Typical optical images of steel balls and sandwich PTFE composites:
(a) PTFE-200#PW-test-20 N-10 Hz,
(b) PTFE500#PW-20 N-10 Hz,
(c) PTFE-500#PWD-20 N-10 Hz,
(d) PTFE-1000#TWD-20 N-10 Hz,
(e) PTFE-200#PW-30 N-20 Hz,
(f) PTFE-500#PW-30 N-20 Hz,
(g) PTFE-500#PWD-30 N-20 Hz,
(h) PTFE-1000#TWD-30 N-20 Hz.

CONCLUSIONS

The COF of PTFE composites decreases with the increases in friction frequency and the wear rate of sandwich PTFE composites decrease with the increase in friction frequency. When the upper PTFE layer is worn out, the bottom PTFE will be squeezed into the friction area under the frictional load. The small contact region can reduce the adhesion of PTFE to the steel ball, resulting in a sudden decrease in COF and a stable COF. At the same time, the wear area will be limited, thereby greatly reducing the wear rate. The wear rate of the middle layer of PTFE-500PW is approximately 50 times lower than that of the upper layer. The middle metal mesh layer has an important impact on improving the tribological performances of PTFE composites. It can improve the thermal conductivity, enhance the strength, and reduce the elastic deformation of composites, and restrict the PTFE to be worn.

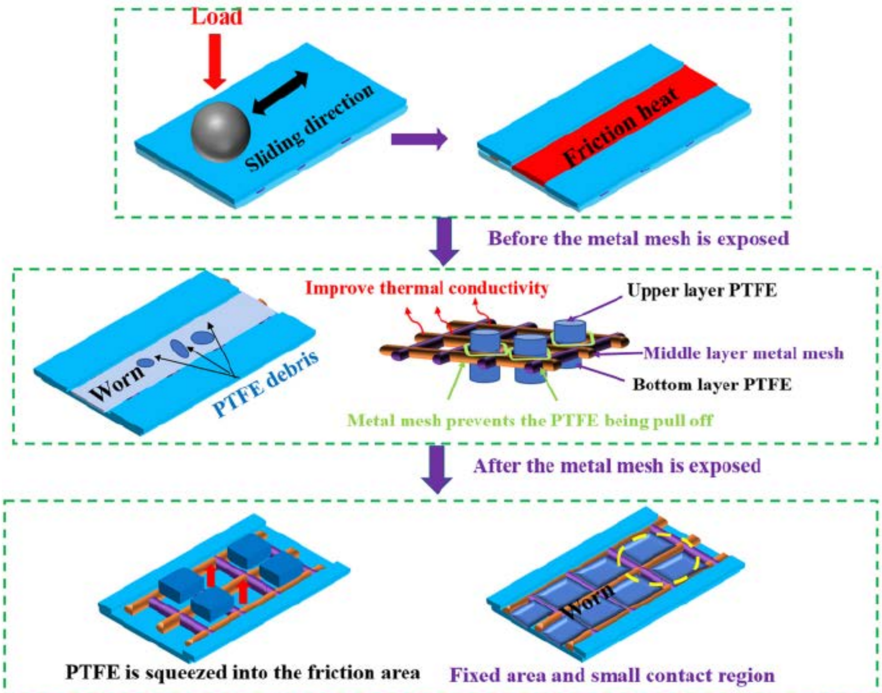

Figure 6: Antifriction and antiwear mechanisms of sandwich PTFE composites.

back to content

REFERENCES

[1] *Qian, M., Song, P., Qin, Z., Yan, S., and Zhang, L. (2019) Mechanically robust and abrasion-resistant polymer nanocomposites for potential applications as advanced clearance joints. Compos. Part A Appl. Sci. Manuf., 126, 105607.*

[2] *Gu, D., Duan, C., Fan, B., Chen, S., and Yang, Y. (2016) Tribological properties of hybrid PTFE/Kevlar fabric composite in vacuum. Tribol. Int., 103, 423–431.*

[3] *Gürgen, S., Çelik, O.N., and Kuşhan, M.C. (2019) Tribological behavior of UHMWPE matrix composites reinforced with PTFE particles and aramid fibers. Compos. Part B Eng., 173, 106949.*

[4] *Shen, J.T., Top, M., Pei, Y.T., and De Hosson, J.T.M. (2015) Wear and friction performance of PTFE filled epoxy composites with a high concentration of SiO2 particles. Wear, 322–323, 171–180.*

[5] *Xiang, D., and Shan, K. (2006) Friction and wear behavior of self-lubricating and heavily loaded metal–PTFE composites. Wear, 260 (9–10), 1112–1118.*

[6] *Xiang, D., Shu, W., and Li, K. (2008) Friction and wear behavior of a new 40Cr steel–PTFE fabric composite under heavy loads. Mater. Sci. Eng. A, 483–484, 365–368.*

[7] *Unal, H., Sen, U., and Mimaroglu, A. (2006) An approach to friction and wear properties of polytetrafluoroethylene composite. Mater. Des., 27 (8), 694–699.*

[8] *Chen, B., Wang, J., and Yan, F. (2012) Synergism of carbon fiber and polyimide in polytetrafluoroethylene-based composites: Friction and wear behavior under sea water lubrication. Mater. Des., 36, 366–371.*

[9] *Ginzburg, B.M., Tochil'nikov, D.G., Lyashkov, A.I., Shiyan, P.A., Gaisin, V.M., Permyakov, I. V., and Ponimatkin, V.P. (2011) Tribological behavior of polyoxymethylene in water-lubricated friction against steel. J. Frict. Wear, 32 (4), 246–250.*

[10] *Liu, S., Li, Y., and Li, N. (2018) A novel free-hanging 3D printing method for continuous carbon fiber reinforced thermoplastic lattice truss core structures. Mater. Des., 137, 235–244.*

[11] *Li, F., Liu, L., Lan, X., Wang, T., Li, X., Chen, F., Bian, W., Liu, Y., and Leng, J. (2016) Modal Analyses of Deployable Truss Structures Based on Shape Memory Polymer Composites. Int. J. Appl. Mech., 08 (07), 1640009.*

[12] *Li, X., Ling, Y., Zhang, G., Yin, Y., Dai, Y., Zhang, C., and Luo, J. (2020) Preparation and tribological properties of solid-liquid synergetic self-lubricating PTFE/SiO2/PAO6 composites. Compos. Part B Eng., 196, 108133.*

[13] *Iyer, S.B., Dube, A., Dube, N.M., Roy, P., and Sailaja, R.R.N. (2018) Sliding wear and friction characteristics of polymer nanocomposite PAEK-PDMS with nano-hydroxyapatite and nano-carbon fibres as fillers. J. Mech. Behav. Biomed. Mater., 86, 23–32.*

[14] *Conte, M., and Igartua, A. (2012) Study of PTFE composites tribological behavior. Wear, 296 (1–2), 568–574.*

[15] *Jia, W., Yang, S., Ren, S., Ma, L., and Wang, J. (2020) Preparation and tribological behaviors of porous oil-containing polyimide/hollow mesoporous silica nanospheres composite films. Tribol. Int., 145, 106184.*

10.1002/app.50803
W. Zhang, X. Li, Y. Zhang, *et al.*
Journal of Applied Polymer Science;

03 Ultra-high-molecular-weight polyethylene: Abrasive wear behavior in a rotating lubricated environment

Adapted from Sun *et al.*, 2022

A study was conducted to explore the effect of the rotation speed on the damage failure mechanism of ultra-high-molecular-weight polyethylene (UHMWPE) in lubricant media containing abrasive particles and in water. The wear mechanism was analyzed by friction coefficient and wear behavior.

Ultra-high-molecular-weight polyethylene (UHMWPE) has excellent engineering properties due to its high molecular weight, including wear resistance, impact resistance, chemical corrosion resistance, etc.[1–3] Therefore, UHMWPE can be widely used in bearings, gears, seals, and wear-resistant materials in petroleum geology, marine equipment, engineering machinery, and other fields.[4,5]

At present, a common approach adopted by researchers to study the tribological properties of UHMWPE materials is using clean water, seawater, and other pure lubricants to set up the environments.[6–8]

It should be noted that some abrasive particles are often mixed in the service environment of UHMWPE, which causes them to be worn by abrasive particles and shorten their service life. Currently, the research on the performance of abrasive wear mainly employs abrasive paper for wear testing, or to demonstrate the superior abrasive wear properties of UHMWPE in comparison to other polymer materials. Previous studies have seldom shown the tribological properties of UHMWPE in lubricated environments with hard abrasive particles, or the mechanisms of abrasive wear in the material. This lack of information is hindering its use as a bearing and sealing structure in industries exposed to abrasive fluids.

This paper uses slurry to establish the abrasive wear environment of UHMWPE and explore the damage mechanism of abrasive particles, providing specific ideas for the enhancement and modification of UHMWPE.

MATERIALS AND METHODS

Test equipment

The friction tests were carried out on an MMW-1 multifunctional friction and wear tester (OuTuo Test Equipment, China). During the tests, a metal disk was fixed in a container with the lubricating medium, then it was brought

◀ back to content

into contact with the polymer sample by the loading mechanism, which was rotated and slid on the surface of the metal disk under the selected rotation speed. Based on the measurement results, the friction coefficient (μ) of the friction pair can be calculated by Equation (1):

$$\mu = \frac{T}{rN} \qquad (1)$$

where T is the torque (N·m), r is the rotation radius of the friction pair (mm), and N is a positive pressure (N). Eventually, the friction coefficient curve was output in real time through the data processing software.

The experiment was carried out considering two lubrication conditions: water and an abrasive-containing lubricating medium. For the configuration of the slurry lubricating medium, we referred to the experimental scheme of Peng *et al.* [9], in which water (94.5% mass fraction), sodium bentonite (600 mesh, 5% mass fraction), sodium carboxymethyl cellulose (0.5% mass fraction), and abrasive sand particles were mixed to form the slurry.

Different rotation speeds were selected to test the tribology performance of UHMWPE materials; the selected test rotation speeds were 240, 300, 360, 420, and 480 r/min in this study. The load applied in the test was 30 N and the corresponding pressure was about 1 MPa. The tribological tests were carried out for 30 min, and each test parameter was repeated at least three times to eliminate potential errors for the reliability of the test results.

Before testing, the UHMWPE specimens were placed in an anhydrous ethanol solution with an ultrasonic cleaner for 5 min to remove the impurities attached to the surface. After cleaning, the specimens were blown dry with cold air and weighed five times; the average value was obtained to get their initial masses. At the end of the test, the UHMWPE pins were cleaned, blown dry, and weighed, in the same manner, to obtain the mass of the UHMWPE pins after wear. Through the calculation of the difference in mass before and after wear, the wear rate (K) can be calculated by Equation (2):

$$K = \frac{\Delta m}{\rho L N} \qquad (2)$$

where Δm is the mass difference of the sample before and after wear (g), ρ is the density of UHMWPE material (g/mm^3), L is the sliding distance (m), and N is a positive pressure (N). The mass loss and wear rate of the lower metal counterparts were obtained in the same way. To ensure the accuracy of the experimental results, we performed at least three tests on each group.

The surface wear morphology of the UHMWPE pin was analyzed by scanning electron microscope (SEM, EM-30, COXEM, Korea), and the chemical compositions on the worn surfaces were detected by using energy dispersive spectroscopy (EDS, Ultim-Max 65, Oxford, UK). Furthermore, the 3D surface profile of the metal counterparts was observed by a confocal laser scanning microscope (OLS4000, Olympus, Japan).

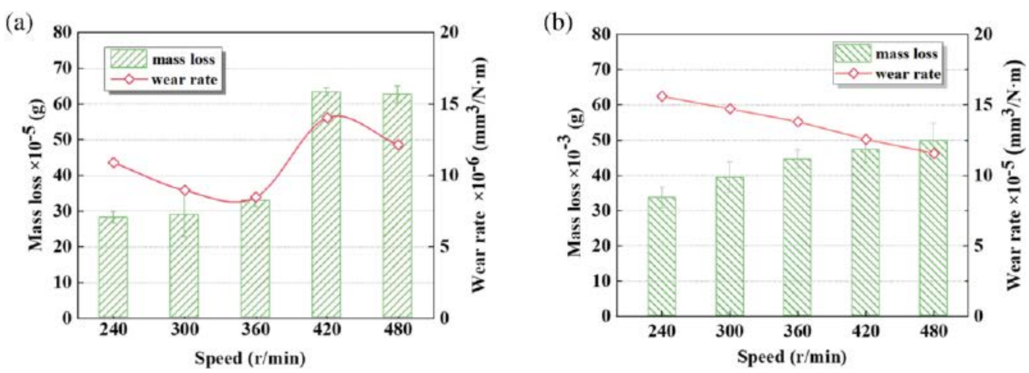

Figure 1: Mass loss and wear rate of friction pairs in the slurry with rotation speed change: (a) UHMWPE; (b) SS304.

◀ back to content

RESULTS AND DISCUSSION

Analysis of friction and wear performance

The average friction coefficient with an abrasive-containing lubricating medium (slurry, 0.15) was higher than that without abrasive (water, 0.05), which reveals that the particles have an important influence on their tribological properties. In addition, the friction coefficient shows different trends in the two environments. The average friction coefficient in the slurry increased gradually with the increased rotation speed. In contrast, the average friction coefficient in the water gradually decreased with the increase in speed, as the lubrication effect of water gradually increased.[10]

For the lubrication environment including abrasive particles, the movement of particles within the interface became more violent as the rotation speed increased. This enhanced the disruption of the integrity of the lubricating water film in the interface by the particles, resulting in direct contact between the two solid surfaces in some places, and the friction pair is in the wear state of wet wear particles, thus increasing the friction coefficient.[11] Notably, the particles have a significant effect on the friction coefficient of the material.

The mass loss of the UHMWPE pin and SS304 metal discs were measured, and the corresponding wear rate in the slurry was calculated as shown in **Figure 1**. The most important thing was that the wear rate of UHMWPE in the slurry environment showed an unusual variation with the increase in rotation speed.

The nonlinear variation of the material wear rate with increasing rotation speed was an anomaly in the present study, and the anomalous variation pattern of wear rate found in previous studies may be caused by the change of the wear mechanism with the change of rotation speed.[12] Therefore, we suspect that different forms of damage may have occurred in the polymer material at different speed stages and that a speed of 360 r/min may be the threshold value for the shift in damage type.

For the SS304 discs, we could see that the mass loss of the mental disc steadily increased with the increase of the rotation speed. The reason for this was that as the sliding distance accumulated, the particles caused an accumulation of damage to the metal counterpart, resulting in an increasing mass loss. However, the wear rate of the metal disc gradually decreased with the increase in the rotation speed. This may be due to the increased lubrication effect of the fluid as the rotation speed increased, which mitigated the wear of the particles on the metal, leading to a decrease in the wear rate of the metal counterparts.

Analysis of worn surface morphology

Figures 2 and **3** show the change in the worn surface of UHMWPE with rotation speed under different lubrication conditions. Particles have a significant impact on the surface wear morphology of the material.

As shown in **Figures 2a,b,** slight cracks and minor plastic deformation on UHMWPE worn surfaces occurred in water lubrication environments, which was very slight wear of the material compared to **Figure 2f.** When the speed gradually increased to 360 r/min, the plastic deformation of the surface protrusion in the original topography was more serious,

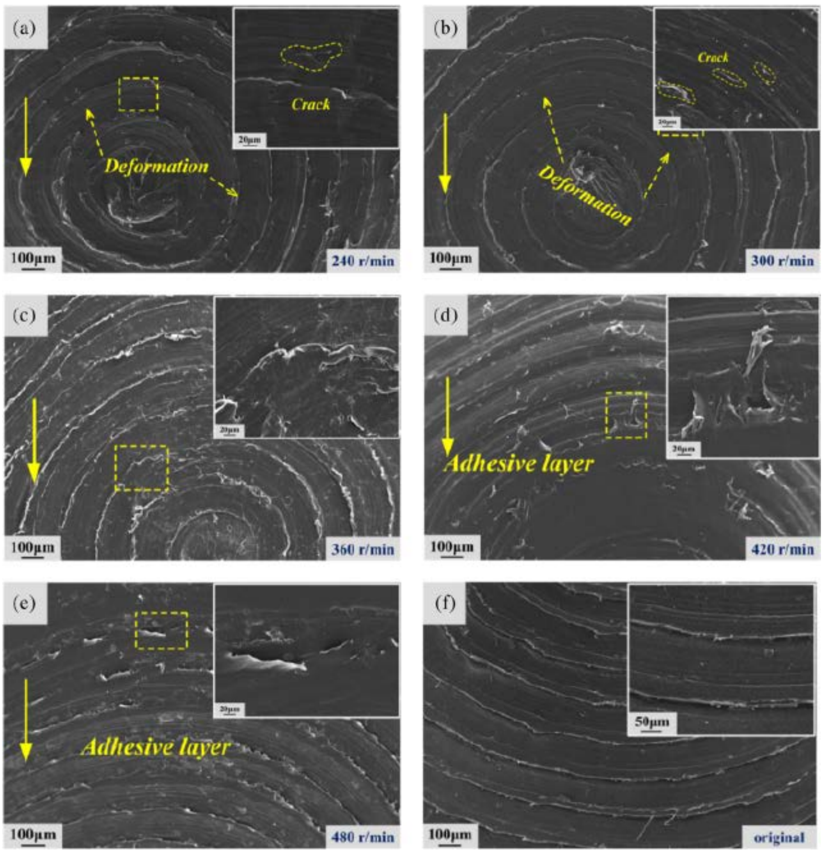

Figure 2: Worn (a-e) and original (f) surface morphology of UHMWPE at different rotation speeds in the water: (a) 240 r/min; (b) 300 r/min; (c) 360 r/min; (d) 420 r/min; (e) 480 r/min.

back to content

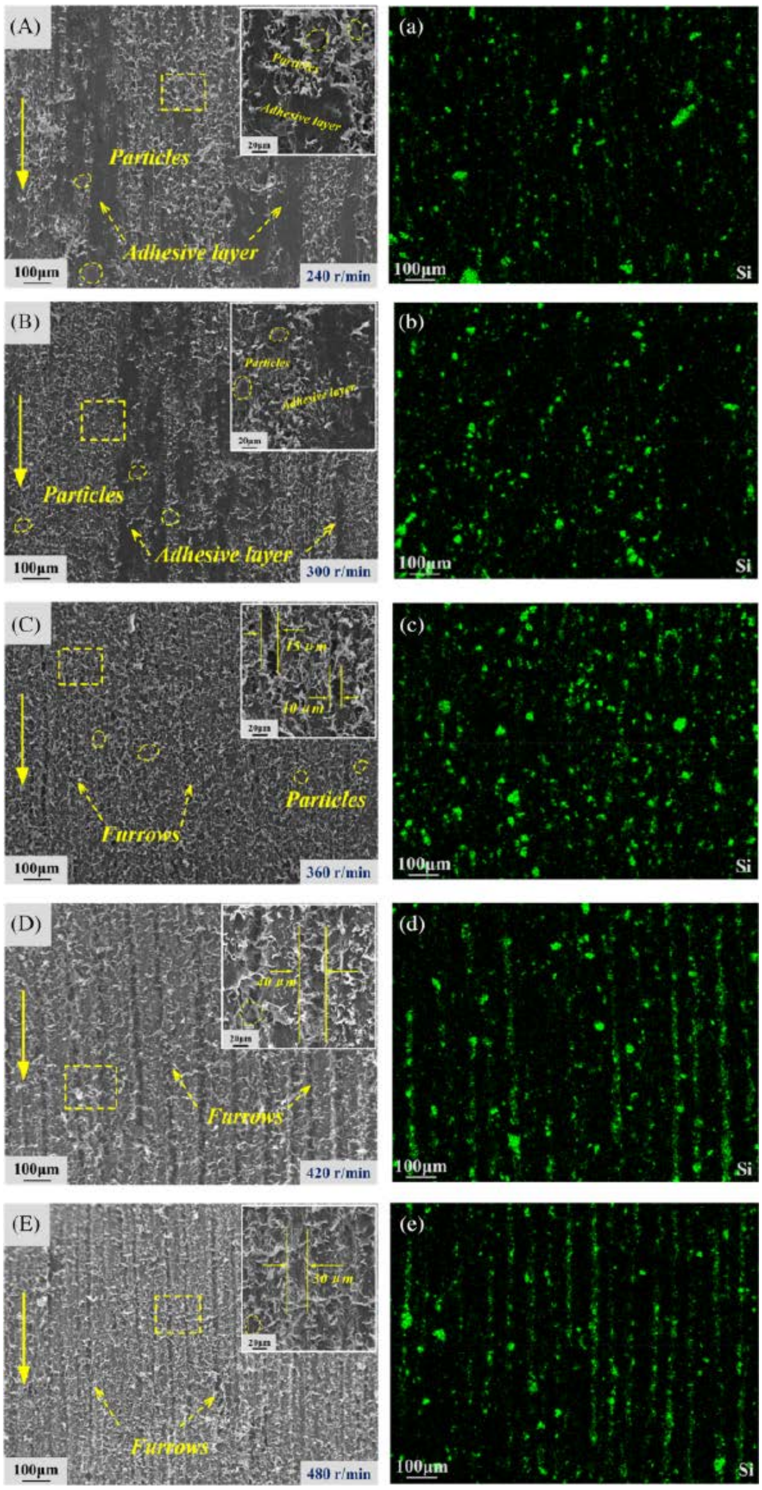

Figure 3: Worn surface morphology (a-e), Si element mapping (a-e) of UHMWPE at different rotation speeds in the slurry: (A,a) 240 r/min; (B,b) 300 r/min; (C,c) 360 r/min; (D,d) 420 r/min; (E,e) 480 r/min

and the protrusion was pushed in the sliding direction under the action of tangential force, exhibiting fatigue wear and with slight adhesive wear. With the speed exceeding 420 r/min, large areas of smooth delamination could be observed on the worn surface.

The change in rotation speed would influence the generation and dissipation of frictional heat, and more frictional heat would be generated with the increase in rotational speed and the accumulation of sliding distance. Since UHMWPE has a low thermal diffusivity, frictional heat is not easily dissipated from the friction interface, and more heat accumulates on the material surface and causes the contact temperature to rise, resulting in thermal softening of the contact interface and lower shear resistance, which eventually forms adhesive wear on the wear surface [13,14] as shown in **Figures 2d,e.**

Interestingly, however, the surface worn morphology of UHMWPE in the slurry was completely different from that of water, which was manifested by the complete disappearance of the original surface shape of the material, as shown in **Figure 2f.** Another point that should not be overlooked was that the damage morphology of UHMWPE was totally different above and below the critical rotation speed.

At the below critical rotation speeds of 240 and 300 r/min shown in **Figures 3a,b,** non-oriented fibrous abrasive chips were clearly distributed on the entire wear surface of the UHMWPE material, which was a typical abrasive wear characteristic. In addition, smooth delamination existed in some areas of the worn surface, which indicated that adhesion was generated on the worn surface during the repeated extrusion of the material. It was also worth mentioning that comparing the silicon element scan images of the worn surface shown in **Figures 3a,b,** we can find a large number of SiO_2 particles embedded in the UHMWPE matrix, especially in the area where three-body abrasive wear occurs in the corresponding SEM. By analyzing these images, we could see that the particles invading the friction interface caused severe abrasive wear on the UHMWPE substrate and also induced fluctuations in the real-time friction coefficient curve.

As the speed reached the critical rotation speed of 360 r/min, embedded abrasive particles and fibrous wear debris generated by particles were apparent on the worn surface, which was shown in **Figure 3C,c.** In addition,

back to content

Figure 4: 3D worn surface morphology and 2D profile curves of UHMWPE in the slurry:
(a) 360 r/min;
(b) 420 r/min;
(c) 480 r/mi

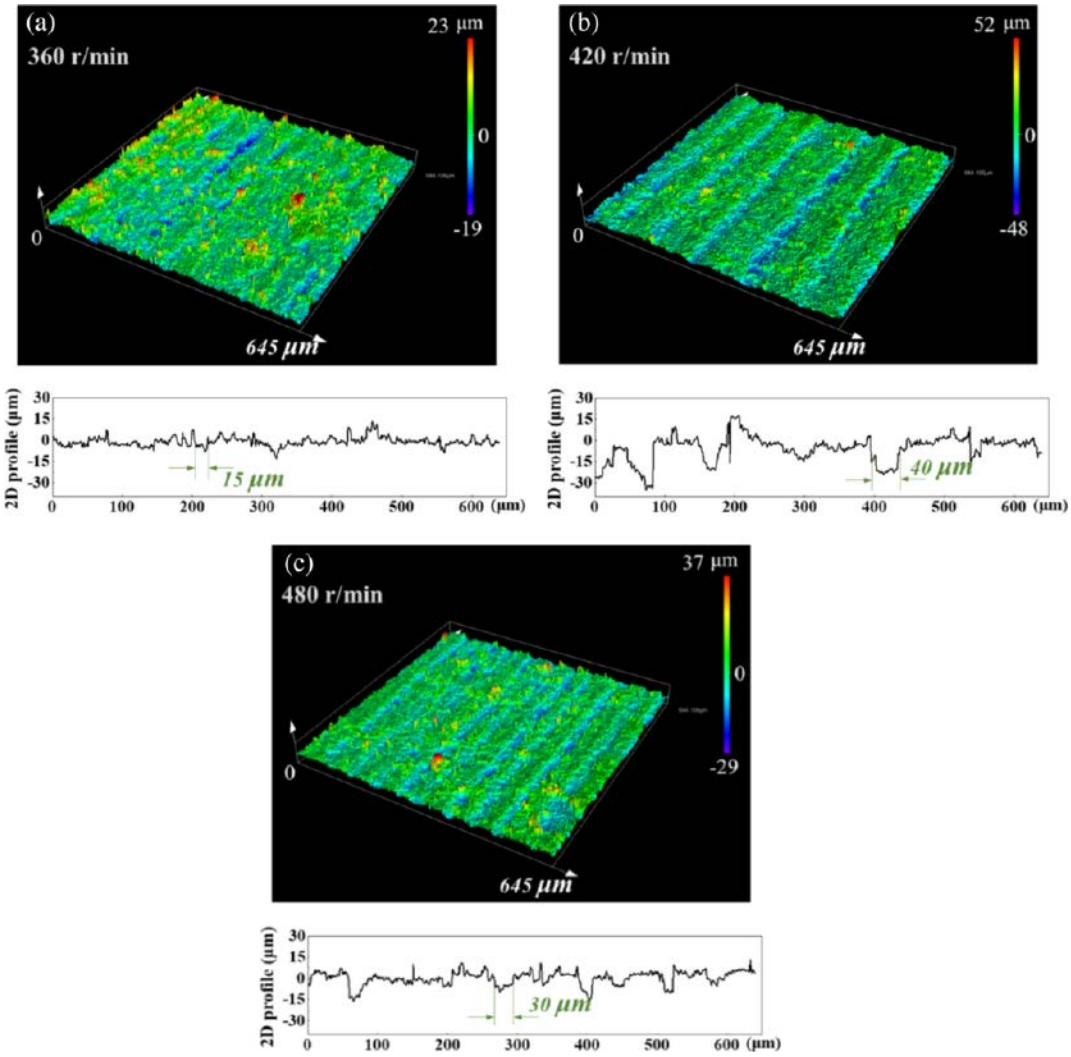

a small number of furrows parallel to the sliding direction were present in the local area on the worn surface of UHMWPE. In order to obtain accurate information on the width and depth of the furrows, we used the confocal laser scanning microscope (OLS5100, Olympus, Japan) to obtain the surface profile of the furrow area, as shown in **Figure 4a**. We found that the width of the furrows on the wear surface could reach about 15 µm, while the depth was only a few microns, and some of the furrows were discontinuous. Therefore, a new form of damage to the material was caused by the abrasive particles in this case. At this speed condition, the plowing effect of the particles was relatively slight, so UHMWPE mainly underwent three-body abrasive wear. **Figure 3c** shows that the high ductility of the material prevented the abrasive chips from falling off from the worn surface, and the abrasion of the particles did not cause severe material removal, thus the wear rate of the material was low under these conditions.

There were a large number of scratches on the metal counterparts along the sliding direction in the lubrication condition of the slurry. Additionally, the rotation speed increased, and the sliding distance accumulated would lead to a gradual widening of the furrows on the metal surface. Specifically, in the middle area of the wear mark, the width of the furrow was about 20 µm when the speed was 240 r/min (**Figure 5a**). When the speed was increased to 360 and 420 r/min, the width of the low furrow was about 50 and 80 µm, respectively. At the corresponding water lubrication condition, the surface of stainless steel was relatively smooth

Figure 5: Worn surface morphology of SS304 at different rotation speeds: (A, B, C) in the water; (a, b, c) in the slurry; and (A,a) 240 r/min; (B,b) 360 r/min; (C,c) 420 r/min

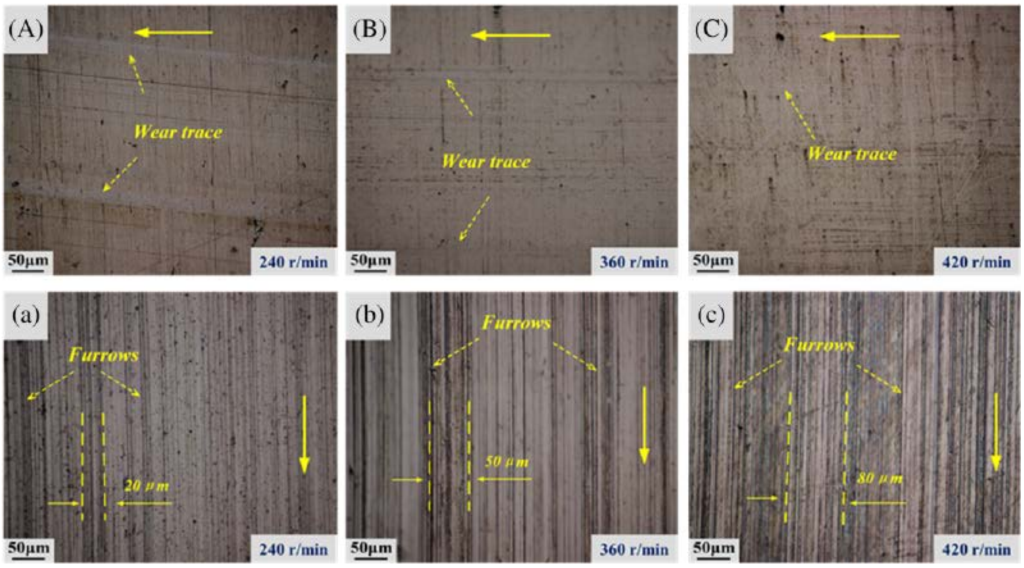

overall, with only slight wear traces observed. With the increase in rotation speed, the wear traces decreased, as shown in **Figures 5a,b,c.**

For visual observation of the worn surfaces of the metal counterparts, the 3D profiles of the metal counterparts at three rotation speed conditions are shown in **Figure 6.** The abrasive particles embedded in UHMWPE at low to medium speed conditions caused significant plowing characteristics on the surface of the metal counterpart and a notable increase in the depth of the furrows on the wear surface. As seen in **Figures 6a,b,** the depth of the furrow increased from about 10 to 20 μm when the rotation speed increased from 240 to 360 r/min. However, the depth of the furrow on the surface of the metal counterpart did not continue to increase when the rotation speed increased to 420 r/min, but rather the

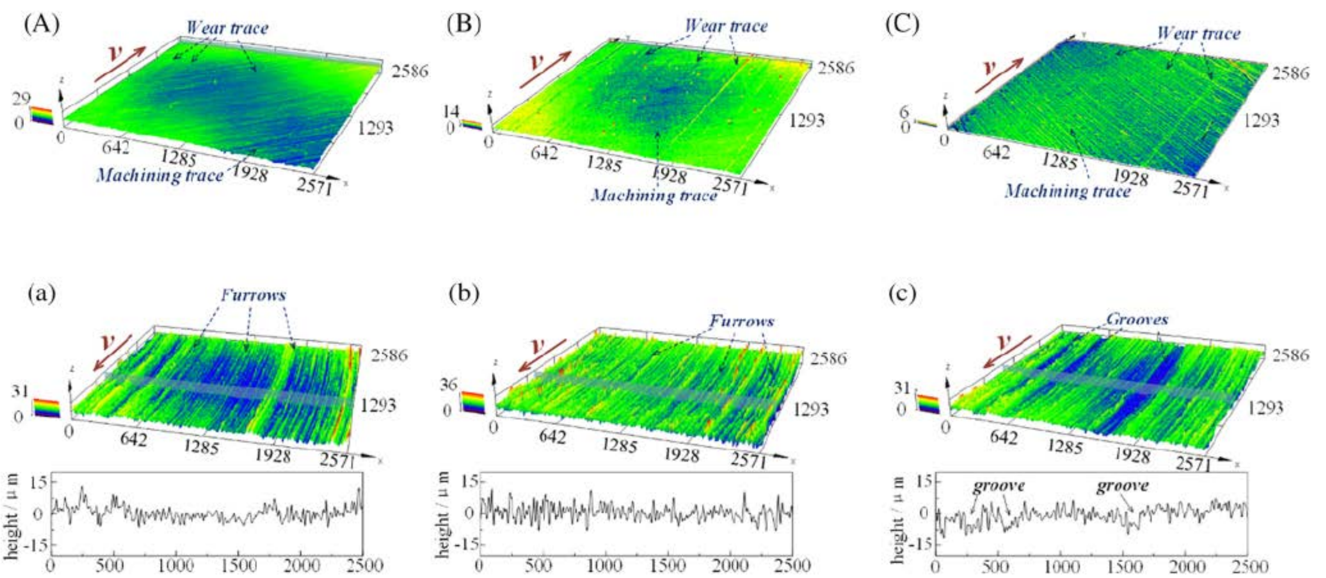

Figure 6: 3D surface profile of the worn surface of SS304 under different rotation speeds: (A, B, C) in the water; (a, b, c) in the slurry; and (A, a) 240 r/min; (B, b) 360 r/min; (C, c) 420 r/min.

back to content

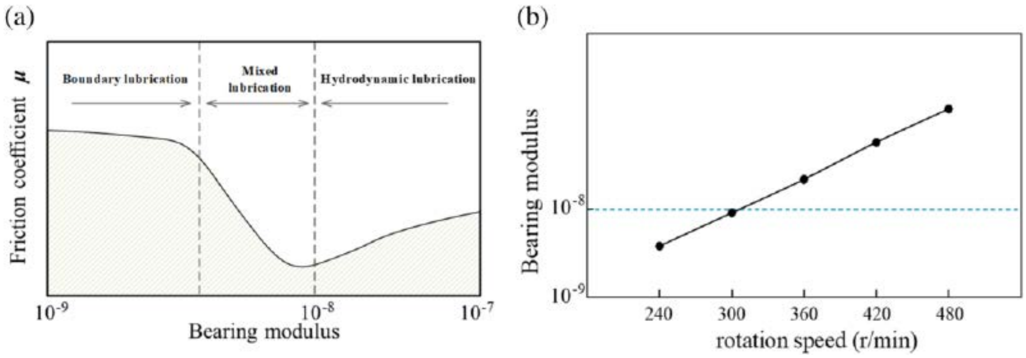

Figure 7: Stribeck curve (a), and the change of bearing modulus with rotation speed (b).

abrasive flow destroyed the ridge of the furrows and formed the grooves on the surface of the metal counterpart, as shown in **Figure 6c.** This indicated that as the speed gradually increased, the accumulated abrasive flow in the furrow continued to wear the metal counterpart mainly by breaking through the ridges of the furrow and not by wearing out deeper furrows. It was the damage to the furrow walls by the particles that caused the wear rate of the metal counterparts to gradually decrease. The surface of the metal counterpart can retain the original machining marks of the surface under the condition of water lubrication, and the worn surface displays slight signs of wear.

Effect of critical rotation speed on wear morphology

By calculating the bearing modulus (ϕ) [15] and comparing it with the Stribeck curve, the results indicated that the lubrication states were mixed lubrication and hydrodynamic lubrication [16], as shown in **Figure 7.** With the increase in rotation speed, the more lubricating medium was brought into the friction pairs to form more stable lubrication, and the lubricating film thickness (*H*) with the increase in speed and gradually increase.[11,17] Moreover, the contact forms of particles in friction pairs were associated with the thickness of the lubricating film.[18] Therefore, an increase in the rotation speed would affect the depth (*h*) of the particles embedded in the soft material within the friction interface.

CONCLUSION

The particles in the slurry caused severe abrasive wear on UHMWPE, which showed different wear characteristics with 360 r/min as the critical speed. The mass loss of UHMWPE doubled when exceeding the critical speed and had the lowest wear rate at the critical rotation speed. UHMWPE exhibits its excellent abrasion resistance in the water.

The wear mechanism of UHMWPE alters when the critical speed is exceeded. Below the critical rotation speed, fibrous debris and an adhesive layer will be formed on the wear surface of the material, and the wear mechanism is three-body abrasive wear and adhesive wear. With the increase of rotation speed beyond the critical speed, the worn surface is mainly characterized by dense grooves parallel to the sliding direction, and the wear mechanism gradually changes to the plowing effect. The wear mechanisms in the water lubrication environment are mainly fatigue wear and adhesive wear.

Based on the change of UHMWPE wear morphology, it was found that the transformation of particle movement mode is the main reason for the change of wear mechanism. The movement mode of abrasive particles on the friction interface changes from being embedded in the HMWPE surface or the rolling cutting predominantly to sliding plowing when the critical speed is exceeded.

back to content

REFERENCES

[1] *Pang, W., Ni, Z., Wu, J., and Zhao, Y. (2018) Investigation of tribological properties of graphene oxide reinforced ultrahigh molecular weight polyethylene under artificial seawater lubricating condition. Appl. Surf. Sci., 434, 273–282.*

[2] *Golchin, A., Wikner, A., and Emami, N. (2016) An investigation into tribological behaviour of multi-walled carbon nanotube/graphene oxide reinforced UHMWPE in water lubricated contacts. Tribol. Int., 95, 156–161.*

[3] *Fu, J., Doshi, B.N., Oral, E., and Muratoglu, O.K. (2013) High temperature melted, radiation cross-linked, vitamin E stabilized oxidation resistant UHMWPE with low wear and high impact strength. Polymer (Guildf)., 54 (1), 199–209.*

[4] *Lin, Y., Guo, Z., and Yuan, C. (2022) Effects of solid lubricants on the tribological behavior of steel-backed <scp>UHMWPE</scp> fabric composites. J. Appl. Polym. Sci., 139 (8), 51674.*

[5] *Chen, S., Wei, L., Cheng, B., Shi, Z., Ding, Y., Zhang, X., and Duan, H. (2022) Effects of thermal-oxidative aging processes on tribological properties of polyformaldehyde and ultra-high molecular weight polyethylene <scp>:</scp> A comparative study. J. Appl. Polym. Sci., 139 (7), 51632.*

[6] *Wang, J., Yan, F., and Xue, Q. (2009) Friction and Wear Behavior of Ultra-High Molecular Weight Polyethylene Sliding Against GCr15 Steel and Electroless Ni–P Alloy Coating Under the Lubrication of Seawater. Tribol. Lett., 35 (2), 85–95.*

[7] *Huang, J., Qu, S., Wang, J., Yang, D., Duan, K., and Weng, J. (2013) Reciprocating sliding wear behavior of alendronate sodium-loaded UHMWPE under different tribological conditions. Mater. Sci. Eng. C, 33 (5), 3001–3009.*

[8] *Belhamdi, H., Kouini, B., Grasso, A., Scolaro, C., Sili, A., and Visco, A. (2022) Tribological behavior of biomedical grade <scp>UHMWPE</scp> with graphite-based fillers against <scp>EBM-Ti6Al4V pin</scp> under various lubricating conditions. J. Appl. Polym. Sci., 139 (23), 52313.*

[9] *Ren, X., Peng, Z., Hu, Y., Rong, H., Wang, C., Fu, Z., Qi, L., and Miao, H. (2014) Three-body abrasion behavior of ultrafine WC–Co hardmetal RX8UF with carborundum, corundum and silica sands in water-based slurries. Tribol. Int., 80, 179–190.*

[10] *Wu, Z., Sheng, C., Guo, Z., Li, Y., Malekian, R., and Li, Z. (2018) Surface texture processing for tribological performance improvement of UHMWPE-based water-lubricated bearings. Ind. Lubr. Tribol., 70 (7), 1341–1349.*

[11] *Dong, C.L., Yuan, C.Q., Bai, X.Q., Yang, Y., and Yan, X.P. (2015) Study on wear behaviours for NBR/stainless steel under sand water-lubricated conditions. Wear, 332–333, 1012–1020.*

[12] *Mao, L., Cai, M., Liu, Q., and He, Y. (2020) Effects of sliding speed on the tribological behavior of AA 7075 petroleum casing in simulated drilling environment. Tribol. Int., 145, 106194.*

[13] *Chang, T., Yuan, C., and Guo, Z. (2019) Tribological behavior of aged UHMWPE under water-lubricated condition. Tribol. Int., 133, 1–11.*

[14] *Gürgen, S., Sert, A., and Kuşhan, M.C. (2021) An investigation on wear behavior of <scp>UHMWPE</scp> /carbide composites at elevated temperatures. J. Appl. Polym. Sci., 138 (16), 50245.*

[15] *Wu, Z., Guo, Z., and Yuan, C. (2021) Insight into water lubrication performance of polyetheretherketone. J. Appl. Polym. Sci., 138 (3), 49701.*

[16] *Zhang, T., Jiang, F., Yan, L., Jiang, Z., and Xu, X. (2021) A novel ultrahigh-speed ball-on-disc tribometer. Tribol. Int., 157, 106901.*

[17] *Yuan, C., Guo, Z., Tao, W., Dong, C., and Bai, X. (2017) Effects of different grain sized sands on wear behaviours of NBR/casting copper alloys. Wear, 384–385, 185–191.*

[18] *sYang, C., Zhou, X., Huang, J., Kuang, F., and Liu, X. (2021) Effects of sediment size and type on the tribological properties of NBR in water. Wear, 477, 203800.*

◀ back to content

04 Tribology and compressive creep of polytetrafluoroethylene/nickel-titanium composites

Adapted from Li *et al.*, 2022

Micro nickel-titanium shape memory alloy particles were incorporated with polytetrafluoroethylene powder by using filling modification technology. The tribological and compressive creep properties of the composites were investigated in detail.

In recent years, polytetrafluoroethylene (PTFE) has been widely utilized in aerospace and aircraft sealing applications.[1,2] However, the high creep and wear rate of PTFE would restrict its use and development in seals where dimensional stability under stress and thermal effects, high-wear resistance, and loading capacity are needed.[3] To utilize the advantages of PTFE and minimize its disadvantages, many kinds of fillers have been applied to develop PTFE-based composites.[4–6] Among the fillers, micro/nanoparticles always showed high efficiency for getting better friction and wear properties.[7,8]

On the other hand, nickel-titanium (NiTi) shape memory alloys, were considered smart functional materials and widely used as biomaterials because of their superelastic behavior. In applications of bearings and gears, the use of NiTi alloy was an effective approach that overcame the limitations of traditional materials.[9]

Here, micro NiTi shape memory alloy particles were incorporated with PTFE powder to develop PTFE composites by using filling modification technology.

EXPERIMENTAL

Preparation of PTFE composites

The PTFE powder used was Daikin M18F suspension resin with a particle size of 1–3 µm and the size of the ellipsoid NiTi particles (VAN-research Institute) was 20–50 µm. The PTFE-NiTi mixture with different mass fractions of NiTi particles (0, 10, 20, 30, 40, and 50 wt%) was dispersed in ethanol. The obtained suspension was mixed in a high-speed mixer (T18 basic Ultra-Turrax, IKA) for 10 min at 9,000 rpm. Then the powders were dried and cold pressed for 10 min by using 10 mm- and 20 mm-diameter cylindrical molds at 10, 20, 30, 40, and 50 MPa, respectively. The compacted specimens were removed from the mold and sintered in ambient air at 340 °C (644 °F) for 1 h with 10 °C/h heating speed and then cooled to room temperature.[10] Before the tribotest experiment, the specimens were polished with 3000# sandpaper and cleaned with petroleum ether, ethyl alcohol, and pure water, respectively. The obtained composites were named after their NiTi content and cold-pressed pressure. For example, 10%–10 MPa composite represents a PTFE composite containing 10 wt% NiTi particles prepared under a pressure of 10 MPa.

Characterization of mechanical and tribological performance

The 10 mm diameter cylinder sample was placed on an electronic universal testing machine (WDW-20/E, Quanlitest) for compressive tests and creep tests. The compressive load was applied at 2 mm/min. The stress and strain of the specimen are given by Equations (1) and (2):

◀ back to content

$$\sigma_e = \frac{F_0}{A_0} \quad (1)$$

$$\varepsilon_e = \frac{(l_0 - l)}{l_0} \quad (2)$$

where, σ_e, ε_e, l_0, and l is the stress (MPa), the strain (%), the initial height, and the instantaneous specimen height (mm), respectively. F_0 is the compressing load (N) and A_0 is the initial cross-sectional area of the specimens (mm^2). Assuming that the specimen volume remains constant during the test, $A \times l$ is equal to $A_0 \times l_0$. Therefore, the true stress (σ_t) and strain (ε_t) can be calculated by Equations (3) and (4).

$$\sigma_t = \sigma_e (1 - \varepsilon_e) \quad (3)$$

$$\varepsilon\_t = -ln(1 - \varepsilon_e) \times 100 \quad (4)$$

The creep tests were carried out at a normal load of 5, 15, and 25 MPa at 30 °C (86 °F), 30 °C, 80 °C (176 °F), and 150 °C (302 °F) for 60 min. The creep strain ε_c was calculated using Equation (5), where ε_1 and ε_2 are the initial and final strain values under the same load.

$$\varepsilon_c = \varepsilon_2 - \varepsilon_1 \quad (5)$$

The tribological performance of the composites was tested using a ball-on-disc tribometer UMT-5 (Universal Micro-Tribometer, Bruker). The disc specimens were PTFE/NiTi composites of 20 mm diameter. A bearing steel ball (GCr15) of 10 mm diameter was used to slide against the PTFE composites. The tests were conducted at a normal load of 10 N, a reciprocating frequency of 10 Hz, and a reciprocating stroke of 6 mm. All friction tests were conducted in an air atmosphere for 20 min and repeated three times. Friction coefficient (COF) values were calculated by averaging the instantaneous COF values. At the end of each test, the wear volume (v) of the composites was obtained using a LEXT 3D measuring laser microscope (OLS5000, Olympus, accuracy: ca. 1 nm), which was equipped with relevant software that can analyze the 3D data and directly show the value. Finally, the wear rate W was calculated using Equation (6):

$$W = \frac{v}{(F \cdot L)} \quad (6)$$

where F is the applied normal load in N, and L is the total sliding distance in m, which was calculated using Equation (7):

$$L = f \cdot 2L \cdot T \quad (7)$$

where f is the reciprocating frequency in the friction test in Hz, l is the reciprocating stroke in m, and t is the ware time in s.

The morphologies of PTFE powders, NiTi particles, and wear tracks of composites were observed and characterized utilizing the LEXT 3D measuring laser microscope, and the scanning electron microscope (SEM, Quanta 200, FEI) equipped with an EDS apparatus.

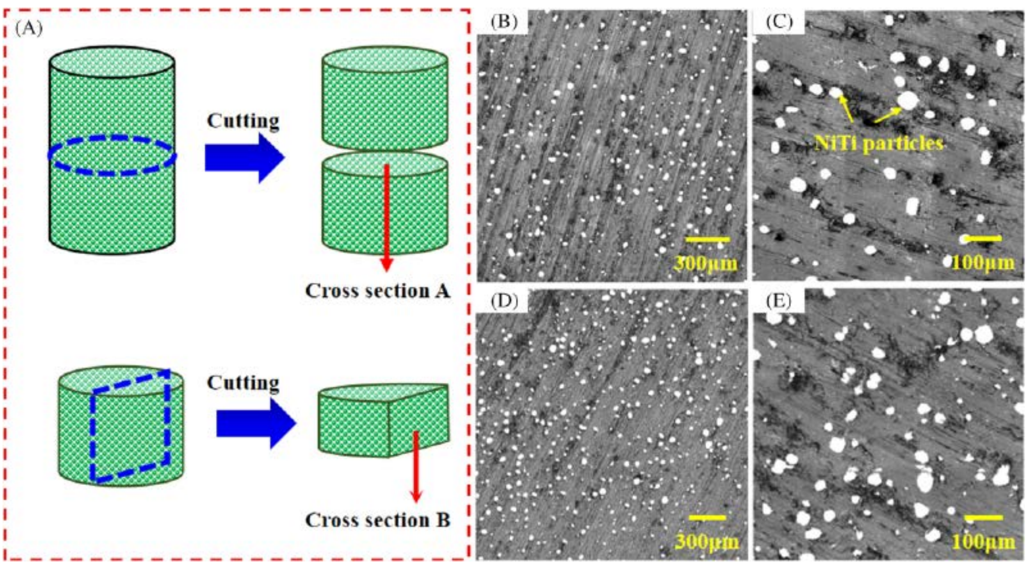

Figure 1: Distribution of NiTi particles inside the PTFE matrix: (A) schematic diagram of specimen cutting, (B) and (C) are low and high-multiple images of section A of composite 30%–30 MPa, (D) and (E) are low and high-multiple images of section B of composite 30%–30 MPa. NiTi, nickel-titanium shape memory alloy; PTFE, polytetrafluoroethylene.

back to content

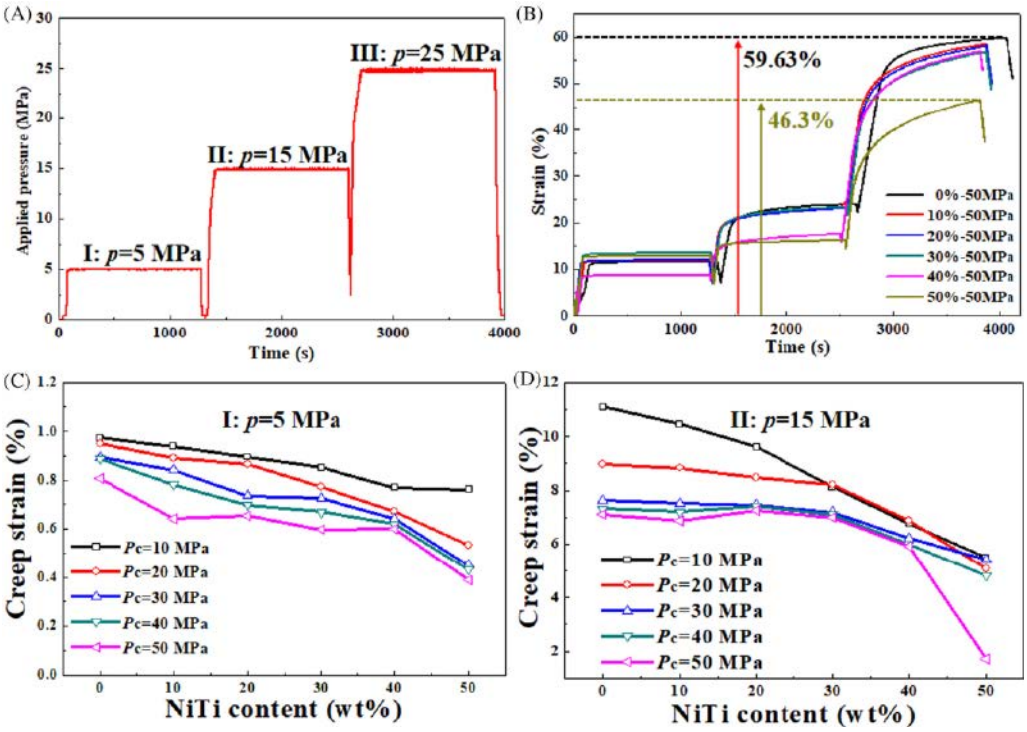

Figure 2: Compressive creep properties tested under changed loads: (A) the compressive pressures applied on the specimen are changed. The applied pressure of stage I is 5 MPa and the load is held for 20 min, the applied pressure is decreased to 0 and then increased to 15 MPa and the load is held for 20 min (stage II), and finally, the applied pressure is decreased to 0 and then increased to 25 MPa and the load is held for 20 min (stage III). (B) Strain-time curves of some composites under the changed loads, (C) the creep strain of composites with the applied load of 5 MPa, (D) the creep strain of composites with the applied load of 15 MPa.

RESULTS AND DISCUSSION

Morphology of particles and composites

SEM images of PTFE powder showed irregular particles of approximately 1–3 μm in size, and NiTi particles near spherical or ellipsoidal with a smooth surface, about 13–52 μm in size. The composites were cut into various parts and the cross sections were observed (**Figure 1**). The prepared NiTi-PTFE mixtures are uniform, dense, and void-free, the NiTi particles are tolerably dispersed inside the PTFE matrix, and more NiTi particles could be found in the cross-section surfaces of composites with larger NiTi content.

Mechanical properties of PTFE/ NiTi composites

The prepared PTFE/NiTi composites had no obvious yield phenomenon, so the stress value corresponding to a strain value of 0.2% was defined as the yield strength. The elasticity modulus and the yield strength of composites increased with the increasing cold-pressed pressure and the NiTi content. NiTi particles, as a kind of hard filler, bear the compressed load and prevent the inter-chain slip of PTFE macromolecules.[11] Therefore, the added NiTi improved the compression strength of PTFE composites.

Figure 2A shows the loading conditions for the compressive creep property test, containing three stages whose loads were 5, 15, and 25 MPa, respectively. The corresponding strain-time curves of some composites are shown in **Figure 2B,** and the creep strains of different composites under various stages were obtained (**Figures 2C-D**). Most of the composites were squashed and the severe plastic deformation happened when the load increased to 25 MPa, therefore the results of creep strains assessed under 25 MPa were not taken into consideration. The strain of neat PTFE material and 50%-50 MPa composite could be as high as 59.63% and 46.3%, respectively (**Figure 2B**). Under the test loads of 5 and 15 MPa (**Figures 2C-D**), the creep strain decreased with the increasing NiTi content and cold-pressed pressure. Moreover, the larger the applied

back to content

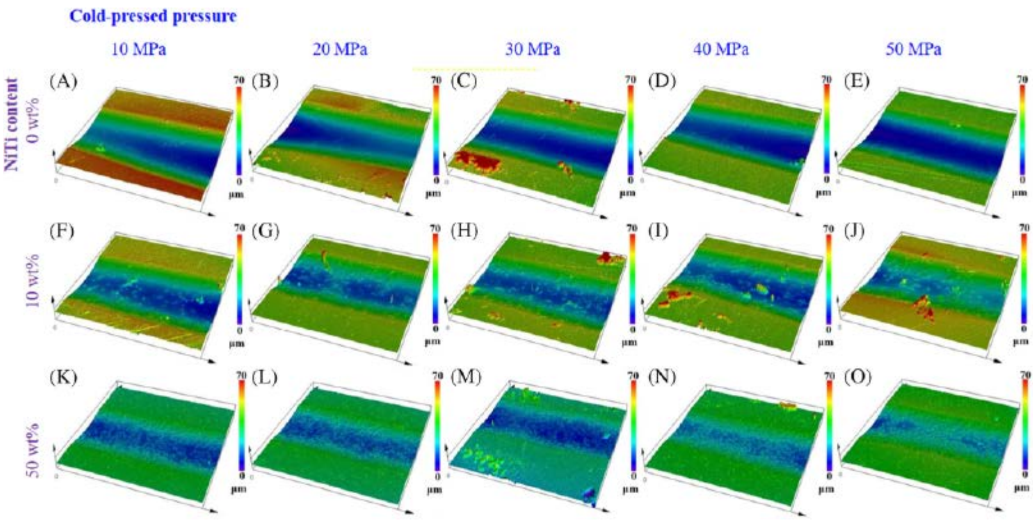

Figure 3: 3D topography of wear tracks on neat PTFE and different PTFE/NiTi composites. NiTi, nickel-titanium shape memory alloy; PTFE, polytetrafluoroethylene.

load, the bigger the creep strain of composites. Under the applied load of 15 MPa, the creep strain of pure PTFE (0%–50 MPa) could be decreased by 75% by adding 50 wt% NiTi particles (50%-50 MPa composite).

Tests of the long-term creep behavior of the composites at different temperatures were conducted. The applied load was 5 MPa and was kept for 1 h. For PTFE/NiTi composites, the creep strain was significantly lower than that of pure PTFE, and the reduction gap became more pronounced as the temperature raised. The creep strain decreased by as much as 60% at 150 °C (302 °F). With the increase in temperature (30 °C to 150 °C or 86 °F to 302 °F), the creep strain first increased slightly and then increased sharply, and the growth trend was slower than that of neat PTFE. Moreover, the higher the cold-pressed pressure and the NiTi content, the smaller the creep strain. The tested PTFE/NiTi composites had smaller creep strain at high temperatures, indicating that NiTi could effectively weaken the movement of molecular chains and reduce creep at elevated temperatures.

Tribological performance of the composites

The COF of PTFE/NiTi was slightly lower than PTFE. With the increase in NiTi content, COF decreased when the NiTi content was no more

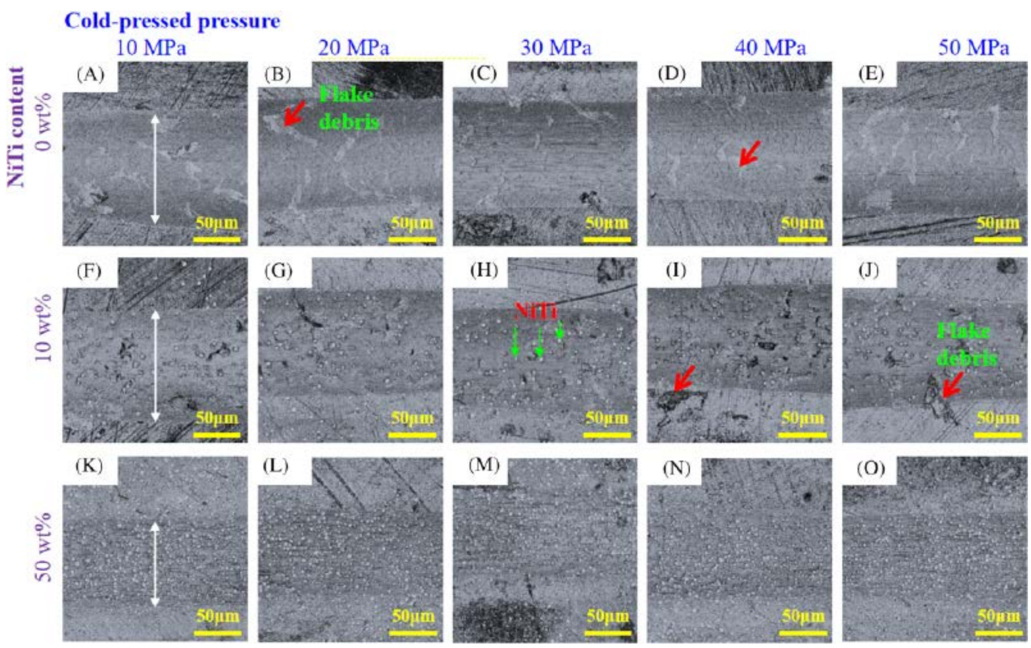

Figure 4: 2D topography of wear tracks on neat PTFE and different PTFE/NiTi composites. NiTi, nickel-titanium shape memory alloy; PTFE, polytetrafluoroethylene.

back to content

than 40%, and the maximum reduction of COF was 7.2%. With the increase in pressure, the COF value decreased, and the maximum reduction was about 5.1%. The minimum COF of all the samples was 0.139 from the 40%–50 MPa composites. The NiTi fillers also enhanced the rigidity and bearing capacity of the composites. The maximum reduction of wear rate was 74% compared to pure PTFE.

Figures 3 and **4** showed the 2D morphology and 3D height morphology of the wear tracks of PTFE/NiTi composites. For pure PTFE (**Figures 3A-E** and **4A-E,** the wear tracks were obvious with bigger depth and width, and there are large, banded debris and pits caused by the peeling of the debris. This indicated that adhesive wear was the dominant wear mechanism of pure PTFE material. For PTFE/NiTi composites, the wear depth became shallower with obvious NiTi particles exposed on the friction surface. The depth of the wear track decreased with the increase of cold-pressed pressure (**Figures 3A-E**) due to the large interface bonding force between NiTi particles and the PTFE matrix, so the PTFE chains were difficult to wear to pieces.

Figure 5 shows the SEM micrographs of worn surfaces of PTFE/NiTi composites. By comparing the wear tracks of 0%–30 MPa, 10%–50 MPa, 30%–30 MPa, and 50%–50 MPa samples, it was found that with the increase of NiTi content, the wear debris changed from macro to micro size. In addition, obvious NiTi particles can be seen on the PTFE/NiTi wear surface, while a small amount of NiTi particles were exfoliated. Compared with the surface of 30%–30 MPa and 30%–50 MPa samples, the wear debris was less and smaller when the cold-pressed pressure is higher, due to the tighter structure of the composite. And when NiTi content increased to 50 wt% (**Figure 5E**), some plow marks can be seen on the wear surface due to the rolling of the NiTi particles. After friction, there are no voids between the NiTi particles and the PTFE matrix, and the NiTi particles function as a small platform to carry the load, which proves that the two are well combined. Meanwhile, the analysis of EDS results at points 1 and 2 in **Figure 5D** showed that a PTFE transfer film existed on the surface of the exposed NiTi particles.

Figure 6 shows the microscopic diagram of the 3D morphology of the wear tracks. The NiTi particles in the abrasion area form distinct microtextures with a certain height. This indicated that the hard NiTi particles would contact and bear the load first. With the increase of NiTi particle content, the spacing and height between the exposed NiTi were reduced. The denser NiTi particles make PTFE debris smaller in size and easier to store in the pits around NiTi particles.

Antifriction and antiwear mechanisms of composites

Since PTFE is a soft material with poor intermolecular bonding ability, it is prone to slip and peel off when subjected to mechanical forces, resulting in severe wear. To improve the wear resistance of PTFE, it is necessary to improve the bearing capacity of the material and minimize the direct contact area between the friction pair and PTFE. **Figure 7** illustrates the possible wear mechanism of PTFE/NiTi

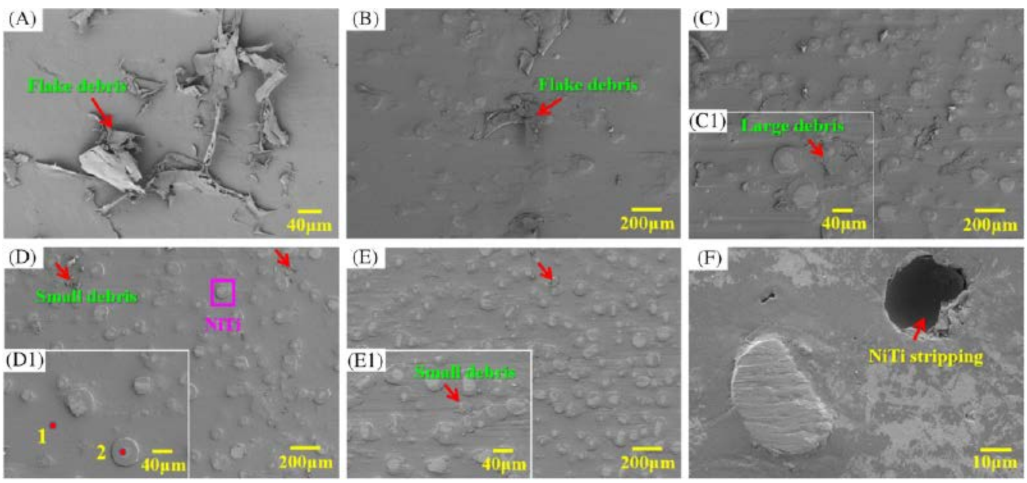

Figure 5: SEM images of wear tracks on different PTFE/NiTi composites:
(A) 0%–30 MPa,
(B) 10%–50 MPa,
(C) 30%–30 MPa,
(D) 30%–50 MPa,
(E) 50%–30 MPa, and
(F) 40%–30 MPa.
NiTi, nickel-titanium shape memory alloy; PTFE, polytetrafluoroethylene; SEM, scanning electron microscope.

back to content

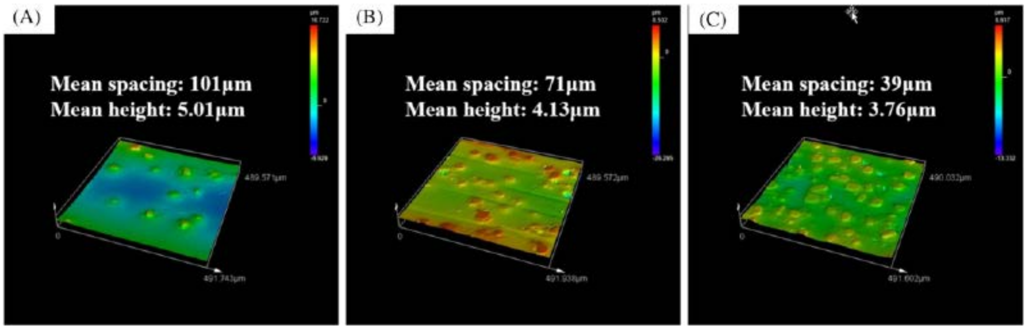

Figure 6: 3D height topography of NiTi particles on wear tracks of different PTFE/NiTi composites:
(A) 10%–30 MPa,
(B) 30%–30 MPa,
(C) 50%–30 MPa.
NiTi, nickel-titanium shape memory alloy; PTFE, polytetrafluoroethylene.

composites. Due to the blocking effect of NiTi particles, large pieces of PTFE fragments are difficult to form. At the same time, the exposed NiTi particles will first contact the friction pair and take priority for bearing the load, which will lower the direct load on the PTFE matrix and reduce the intermolecular shear and wear of PTFE. In addition, a thin PTFE transfer film will be formed on the upper surface of exposed NiTi particles during the friction process, which is conducive to the formation of a stable friction system and the reduction of wear on friction pairs. Moreover, when the NiTi content increases, the friction pair encountered more NiTi particles, thus reducing the contact area with PTFE and further preventing the load transfer on PTFE. The grinding debris will be more easily and stably stored in the pits around NiTi particles without being taken away, thus reducing the wear.

CONCLUSION

The compressive strength and creep resistance of the PTFE/NiTi composites were improved with the increasing of NiTi particle content, and the creep strain of PTFE/NiTi composites can be reduced by up to 60% at 150 °C (302 °F), which indicated that the presence of NiTi particles could effectively limit the active space of PTFE molecular chains and enhance the creep resistance. Moreover, with the increase of NiTi particle content (less than 50 wt%), the COF decreased. Also, the wear rate decreased with the increase of NiTi particle content and cold-pressed pressure. Eventually, based on the morphology of wear tracks, the contact between the counterpart ball and PTFE/NiTi composites was reduced due to the gradual exposure of NiTi particles with a preferential bearing effect, resulting in the improvement of antiwear performances.

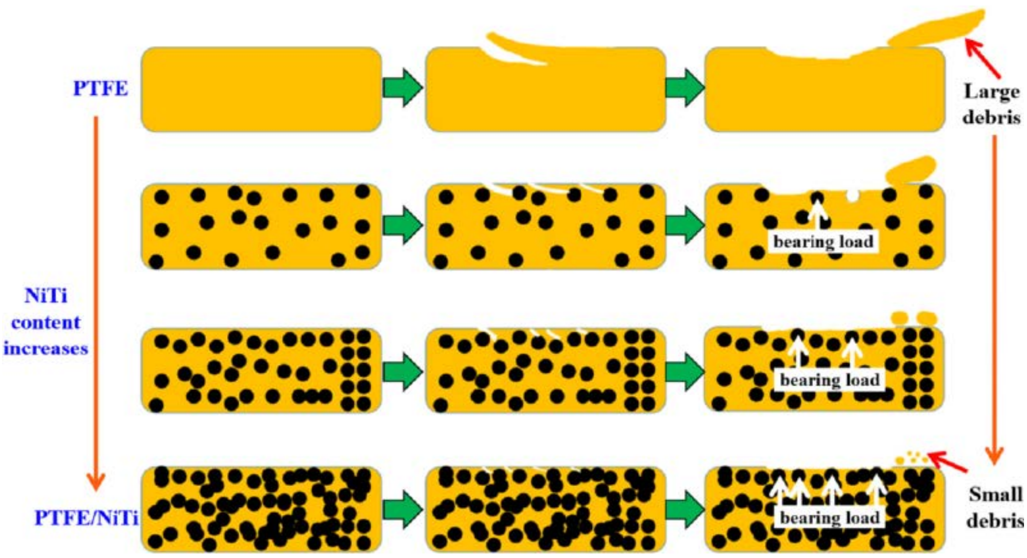

Figure 7: Antifriction and antiwear mechanisms of PTFE/NiTi composites. With the increase of NiTi particle content, the antiwear performance improves. NiTi, nickel-titanium shape memory alloy; PTFE, polytetrafluoroethylene.

back to content

REFERENCES

[1] *Johansson, P., Marklund, P., Björling, M., and Shi, Y. (2021) Effect of humidity and counterface material on the friction and wear of carbon fiber reinforced PTFE composites. Tribol. Int., 157, 106869.*

[2] *Sawae, Y., Morita, T., Takeda, K., Onitsuka, S., Kaneuti, J., Yamaguchi, T., and Sugimura, J. (2021) Friction and wear of PTFE composites with different filler in high purity hydrogen gas. Tribol. Int., 157, 106884.*

[3] *Sahli, M., Cablé, A., Chetehouna, K., Hamamda, S., Gascoin, N., and Revo, S. (2017) Preparation and characterization of polytetrafluoroethylene (PTFE)/Thermally Expanded Graphite (TEG) nanocomposites. Compos. Part B Eng., 124, 175–181.*

[4] *Xie, T., and Shi, Y. (2021) Effects of LaF3/CeF3 on the friction transfer of PTFE-based composites. Tribol. Int., 161, 107069.*

[5] *Li, X., Wu, S., Ling, Y., Zhang, C., Luo, J., and Dai, Y. (2020) Preparation and tribological properties of PTFE/DE/ATF6 composites with self-contained solid-liquid synergetic lubricating performance. Compos. Commun., 22, 100513.*

[6] *Wang, Z., Kou, K., Liu, Z., Zhang, D., Bi, H., Chao, M., and Zhao, Q. (2012) Structural characterization and high-temperature compressive creep of PTFE-based composites filled with inorganic nanoparticles. Polym. Adv. Technol., 23 (3), 545–550.*

[7] *Luo, F., Tang, B., Yuan, Y., Fang, Z., and Zhang, S. (2018) Microstructure and microwave dielectric properties of Na1/2Sm1/2TiO3 filled PTFE, an environmental friendly composites. Appl. Surf. Sci., 436, 900–906.*

[8] *Park, M.S., Sung, H.-S., Park, C.H., Han, T.-S., and Kim, J.H. (2019) High tribology performance of Poly(vinylidene fluoride) composites based on three-dimensional mesoporous magnesium oxide nanosheets. Compos. Part B Eng., 163, 224–235.*

[9] *Sun, W., Liu, X., Liu, K., Wang, W., and Ye, J. (2020) Ultralow wear PTFE composites filled with beryllia and germania particles. Wear, 450–451, 203270.*

[10] *Li, X., Ling, Y., Zhang, G., Yin, Y., Dai, Y., Zhang, C., and Luo, J. (2020) Preparation and tribological properties of solid-liquid synergetic self-lubricating PTFE/SiO2/PAO6 composites. Compos. Part B Eng., 196, 108133.*

[11] *Bahadur, S., and Gong, D. (1992) The action of fillers in the modification of the tribological behavior of polymers. Wear, 158 (1–2), 41–59.*

◀ back to content

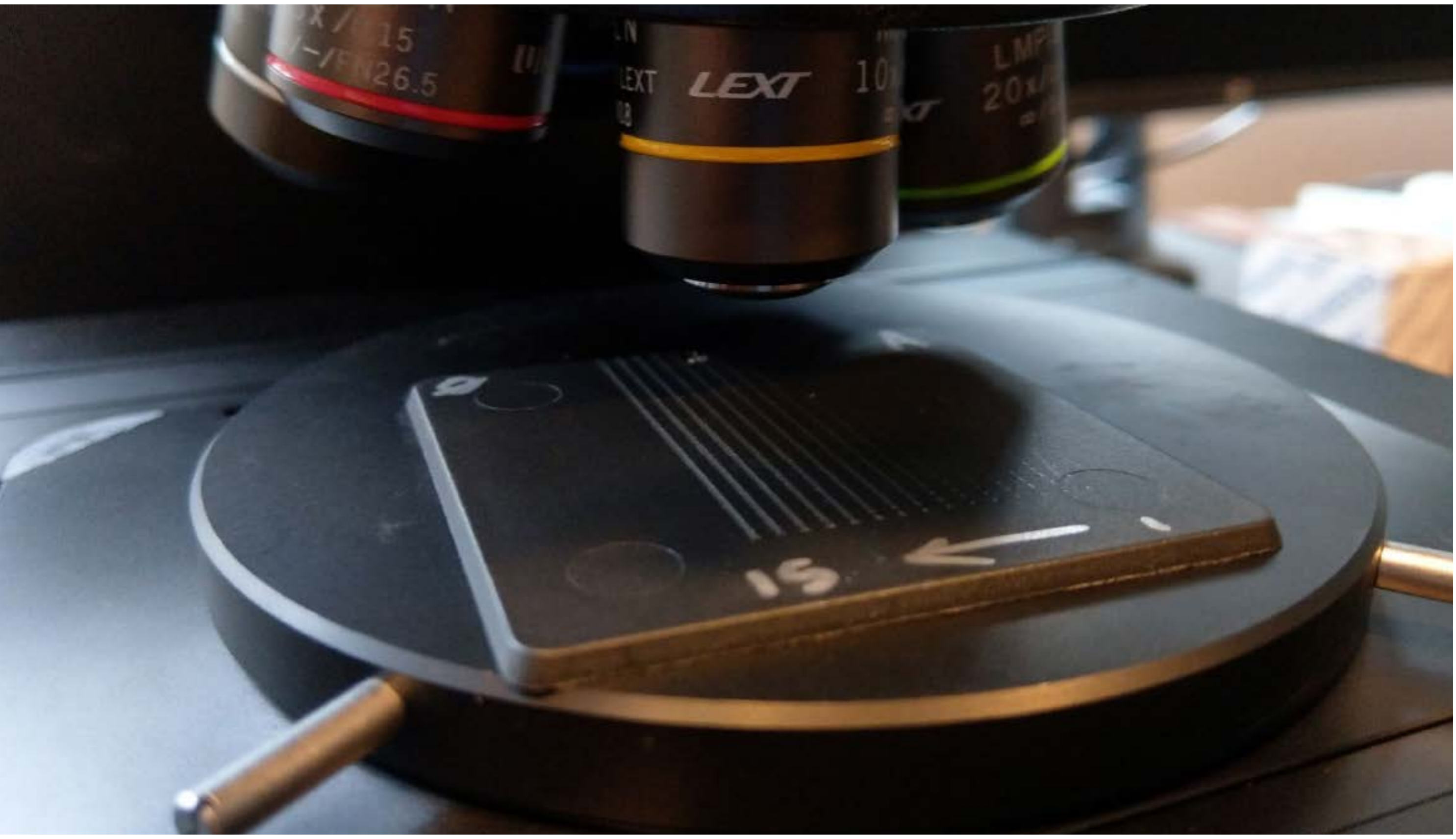

Fast, accurate scratch measurements on polymer plaques with the LEXT OLS5000 microscope

05 Getting up to scratch with Croda – testing anti-scratch additives for polymer plastics

By Sarah Williams

As new car owners can attest, the first time their vehicle gets scratched or damaged is usually the most distressing. Maintaining a car's appearance is not only about aesthetics, it's also about resale or trade-in value. To help prevent unsightly scratches and minimize damage to cars' plastic components, automobile manufacturers rely on scratch-resistant polymer plastics for their injection molded parts.

Enter Croda International PLC—a leading producer and supplier of additives that improve scratch resistance in plastics. An important part of Croda's process is to accurately measure how much these additives improve resistance using scratch tests.

Croda scientists seek a more efficient and precise scratch-test tool

Scientists at Croda had been using a wide-field materials microscope to measure a scratch's width and a white-light interferometer to determine the depth – but they found these methods to be time-consum-

back to content

ing and variable. In a bid to improve testing, Croda decided to try our LEXT™ OLS5000 confocal microscope for both the scratch width and depth measurements.

We spoke to Martin Read, team leader for Croda's polymer additives applications and lead anti-scratch scientist, and his colleagues to find out how it went.

A day in the life of an anti-scratch scientist

The job of an anti-scratch scientist at Croda involves producing plastic plaques containing various additives and then damaging them with numerous scratches! Of course, this needs to be controlled, so these scratches are made with a standardized tool at defined forces of 1–20 newton (N).

"It leaves a scratch and two mounds on either side, similar to a plough going through a field," says Martin.

After the scratching, the researchers measure the depth, width, and profile of the plaques to determine the extent of the damage to each and the differences between them.

Advantages of laser scanning confocal microscopy over interferometry

Hoping to get more precise data and to speed up the workflow, researchers tried the OLS5000 confocal microscope as the sole equipment to measure scratch width and depth. The LEXT microscope's laser has a fast scan speed, enabling it to quickly create precise, quantifiable 3D maps of a sample.

Croda researchers found that imaging, measurement, and analysis were much quicker using the OLS5000 microscope. In fact, their inspections were 10 to 100 times faster compared to interferometry. Martin explains, "To measure a scratch, we had to set up the interferometer to its coarsest setting, and configuring that is extremely difficult. It takes about an hour to get one measurement. With confocal microscopy we could measure and process 10 scratches on a plastic surface in 2 minutes."

The scientists were also pleased to find that the LEXT microscope helped improve the precision of results – scratch depth and profile could be measured to the nearest 10 nm. According to Martin, "because the LEXT can accurately measure in 3D we could simply view a slice through the scratch and measure depth much easier."

The LEXT microscope even managed to come to the rescue with tricky materials like polypropylene. As Martin explains, "polypropylene has a porous structure – the interferometer does not detect the surface – it looks straight through it." Using the LEXT OLS5000 microscope, the scientists were able to obtain a smoother image of the surface and an accurate representation of the scratch, which they could then measure more precisely.

Good news for Croda, means good news for the automotive industry

Croda determined that the LEXT microscope helped improved their inspections, reporting both increased speed and accuracy. As Martin's colleague Dimitris Vgenopoulos, applications scientist, puts it, "seeing how fast the Olympus microscope is, it's almost annoying to think how much time I've spent using the old system."

This improvement in performance is good news for automobile manufacturers and, consequently, car owners. The LEXT OLS5000 microscope helps ensure accurate inspection of these important additives, so you can rest assured that your new car will be up to scratch!

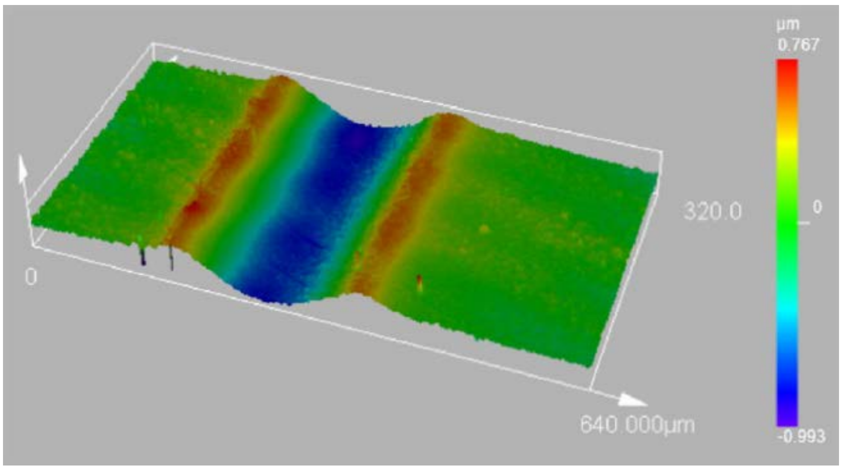

Detailed 3D maps without artifacts make it easier to determine all the parameters.

Read the full case study **here.**

back to content